The Effect of Tritium-Induced Damage on Plastic Targets from High-Density DT Permeation

Introduction

Direct-drive inertial fusion experiments on LLE's OMEGA Laser System[1] and indirect-drive experiments at Lawrence Livermore National Laboratory's (LLNL's) National Ignition Facility[2] use glow-discharge polymer (GDP) as the capsule material that contains the cryogenic DT fusion fuel.[3] Knowledge of the outside diameter of the capsule and the fuel layer's thickness and uniformity are critical so that appropriate laser conditions can be set for the implosion experiment.

Cryogenic targets measured in the cryogenic target Characterization Stations have had greater than expected outside diameters (OD's) (up to 13 μm) from thermal contraction after cooling. The expected diameters were calculated from the General Atomics' (GA's) National Institute of Standards and Technology (NIST)-traceable, room-temperature–measured OD value and the coefficient of thermal expansion of GDP; this contraction was not observed. As a secondary effect, mismeasurement of the OD can influence the reported fuel-layer thickness. To examine this effect, several experiments were performed including (1) an optical system calibration check; (2) a comparison of OD's measured in the cryogenic system with a NIST-traceable value (864.1±0.5-μm-OD silicon ball measured at GA); (3) a parametric study of how system variables can affect the OD measurement; and (4) a comparison of an opaque sphere versus a transparent sphere.

Experimental Configuration

1. Optical System Description

Cryogenic targets are characterized[4] using the non-telecentric, *f*/5, long-working-distance objective shown in Fig. 151.35. The target is illuminated with a pulsed 630-nm-wavelength light-emitting diode (LED) to minimize the effects of target vibration. This wavelength, along with the *f*/5 optics, gives a diffraction-limited (Rayleigh criterion) resolution of 3.8 μm. A 1000 × 1000-sq-pixel, 12-bit charge-coupled device (CCD) is used to record an image of the target. This gives a 1-μm pixel size given the 1-mm object-space field of view; the image is oversampled and there is no loss in resolution resulting from the pixel size.

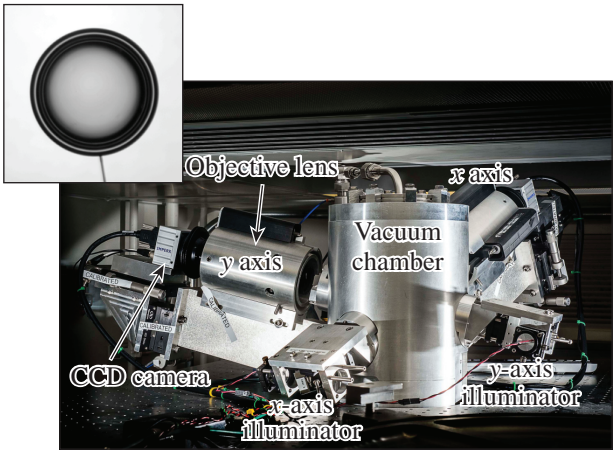

E26202JR

Figure 151.35
Characterization Station used to determine the thickness and uniformity of the solid DT layer. The fuel is layered in a cryogenic enclosure ("layering sphere") filled with He gas that transports heat caused by beta decay of the DT from the capsule. A layered capsule mounted on a SiC fiber is shown in the inset. CCD: charge-coupled device.

2. Image Analysis

The optical system is calibrated (μm/pixel) with a "grid target" that consists of an array of opaque 10-μm-diam aluminum dots that are 20 μm apart on center to within 0.1 μm (see Fig. 151.36). The distortion of the image and centration of the optical axis of the imaging system are also measured and corrected, if necessary, using this grid. Periodic confirmation of calibration using the grid target is performed, especially after any changes are made to the optical path of the system, such as replacing windows or adjusting the optical axis.

To find the outside diameter, 360 radii of the target's image are traced from the center of the capsule. The region where the intensity transition from dark to light is analyzed, the locations where the intensity begins to transition from the local minimum to the local maximum are determined, and the halfway point between them is deemed the perimeter of the target. [See Fig. 151.39 (p. 162) for an example of a radius versus angular position plot.] The target's radius is then calculated using the

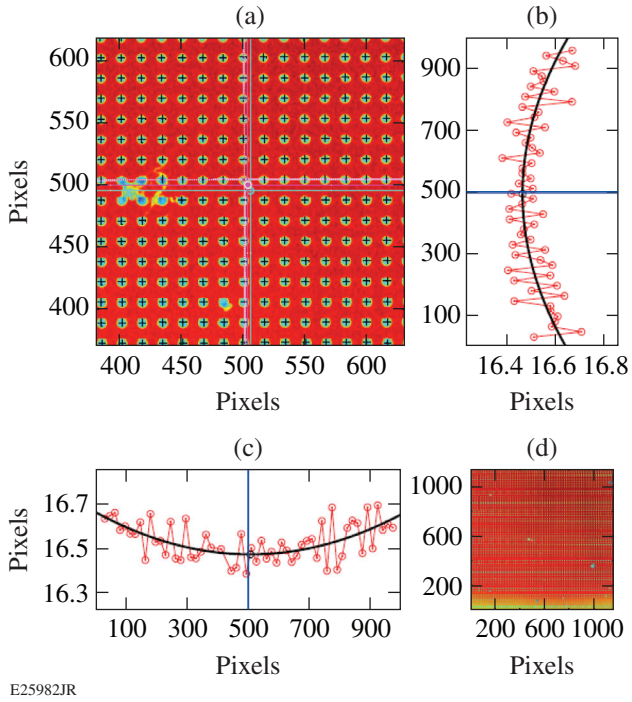

Figure 151.36
Typical calibration images for the Characterization Stations; the image in (a) is the central region of the entire field shown in (d). The locations of the dot centers are compared to the known spacing to calibrate the optical system. Plots used to correct distortion are shown on each side of the central region; the pixel spacing between dot centers is plotted as a function of position in the field for the (b) vertical and (c) horizontal directions. In addition, the optical system is adjusted to remove any skew in these plots to ensure that the capsule is centered on the objective's optical axis.

calibrated μm/pixel value; the OD is given by doubling that number. The diffraction-limited resolution of the optical system is 3.8 μm, but the radius is sampled every degree (360 times) around the perimeter (with some measurements discarded because of the stalk). The theoretical uncertainty in the measured radius could be as low as $3.8/\sqrt{360} = 0.2$ μm. This is doubled when quoting the diameter, so agreement to 0.5 μm should be expected. The diffraction limit is seldom achieved in real systems, however, because of additional sources of aberration such as spherical aberration produced by viewing through the vacuum windows.

Calibration Verification

1. Optical Calibration Confirmation

A grid target (manufactured by Applied Image[5]) identical to the one currently being used with the Characterization Stations was measured with a compound microscope that had been calibrated using a Nikon stage reticule. It was the same grid target that was used when evaluating the cryo target characterization technique off-line during the technique's development. The accuracy of the microscope was also confirmed by correctly measuring a NIST-traceable, standard 1-mm-diam ball.

Using the traveling stage, 30 dots traversed the eyepiece cross hairs in both the x (parallel to stalk) and y (perpendicular to stalk) directions. The measured distances of x = 599.8 μm and y = 599.2 μm give a dot pitch in the x direction of 19.99 μm and in the y direction of 19.97 μm, which agrees with the manufacturer's quoted pitch of 20.0±0.1 μm.

2. Analysis Software Confirmation

To examine the reliability of the analysis software, synthetic data were generated and analyzed with the program. The analysis software reproduced exactly the quantities used to produce the synthetic data.

Possible Sources of Error in OD Measurement

Several parameters were varied to determine their effect on the measured outside diameter as summarized in Table 151.II.

Table 151.II: Effects of parameters studied on the measured OD of the Si ball.

Parameter studied	Effect
Illumination intensity	Effect if background is saturated
Illumination geometry (numerical aperture)	No effect
Focus shift	Effect only if image is conspicuously out of focus
Position of the capsule along the optical axis of the imaging system (image refocused)	No effect
Position of the capsule laterally in the field of view	No effect
Characterization station	No effect
Moving Cryostat Transfer Cart	No effect
Opaque versus transparent sphere	No effect

1. Image Illumination

We first studied the saturation of the camera surrounding the capsule's image and its effect on the diameter reported by the software analysis. A GA-measured (864.1±0.5-μm-outer-diam) silicon (Si) ball was measured using Characterization Station #3. Examples shown in Fig. 151.37 give the measured outside diameters and LED currents that produced the images.

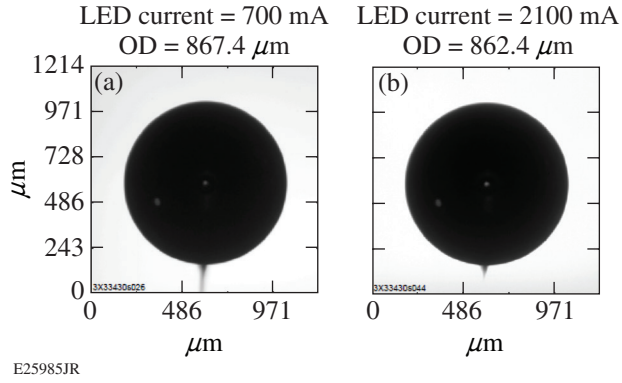

Figure 151.37
Change in apparent diameter of the Si ball resulting from saturation of the camera surrounding the capsule's image. The diameter reported by the software analysis and light-emitting diode (LED) current of the illumination diode is given for (a) a properly illuminated image and (b) an image with a saturated background.

It was noted at this point in the study that the program is reporting a slightly larger OD (867.4 μm) even with appropriate illumination.

The effects of illumination were then tested with a poly α-methyl styrene (PAMS) capsule with a GA-reported outside diameter of 867.4 μm (wall thickness = 19.2 μm). Results for the x-axis view are shown in Fig. 151.38 along with the LED currents that produced the images. In Fig. 151.38(a), when properly illuminated so that the full dynamic range of the camera is utilized, the OD of the x axis is 869.2 μm and the OD of the y axis is 871.2 μm. Figure 151.38(b) is underilluminated and the OD is slightly overestimated: x-axis OD = 869.4 μm; y-axis OD = 871.6 μm. Figure 151.38(c) is clearly saturated and the OD is significantly underestimated: x-axis OD = 862.2 μm; y-axis OD = 859.8 μm. The program is still reporting a slightly larger OD even with proper illumination. Note that the x-axis OD is closer to the GA value than the y-axis OD with proper illumination. The source of this discrepancy is unclear since the Si ball's OD measured the same in both axes. It may be an effect of the capsule's transparency and the illumination nonuniformity present in the frame; this is evident in the offset central bright region inside the capsule's image.

The error in Fig. 151.38(b) may be caused by noise in the image that is clearly visible in the capsule's darker periphery; note that the error is small when compared with Fig. 151.38(a). The OD in Fig. 151.38(c) was underestimated because of "blooming." At saturation, pixels lose their ability to accommodate additional charge. This additional charge will then spread into neighboring pixels, causing them to either report erroneous values or also saturate. This spread of charge to adjacent pixels is known as blooming.

To prevent saturation, the pixel values in the background of the image are displayed by the software in real time by analyzing the image. After it is confirmed that the image is not saturated, data are recorded and analyzed. Only images with the correct illumination are collected for analysis; other than the systematic error of an ~3-μm overestimate of the OD, image illumination is not the source of OD discrepancy.

2. Illumination Geometry

Another test to see if the OD measurement was sensitive to the illuminating ray bundle was performed by adjusting the illuminator's aperture to control the distribution of the rays coming from the light source. Three aperture conditions were tested: 100%, 50%, and 10% open. The 10%-open condition produced distinct diffraction rings around the image of the Si ball, whereas the others only reduced the intensity of the image. The intensity was adjusted to give the same background intensity for each condition, and images were captured and evaluated. All gave the same OD value as previous experiments: the measurement overestimated the OD by about 3 μm.

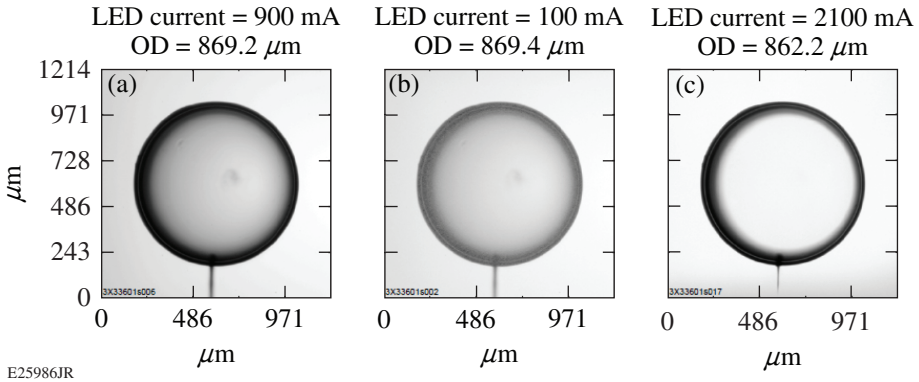

Figure 151.38
Effect of illumination intensity on the apparent diameter of the poly α-methyl styrene (PAMS) capsule. The diameter reported by the software analysis along the x viewing axis and the LED current of the illumination diode are given for (a) a properly illuminated image, (b) an underilluminated image, and (c) an image with a saturated background.

3. Focus Shift

Since the imaging systems in the Characterization Stations are not telecentric, the apparent diameter changes with focus adjustment. When examining the target's surface for debris, the focus is shifted by several hundred micrometers. Returning to the "best focus" after these adjustments is subjective and may be operator dependent. In addition, the target can move in and out of focus because of vibration around its best-focus position.

An experiment was performed to test the effect of moving the Si ball out of the focal plane while holding the objective's focal plane fixed; these results are summarized in Fig. 151.39. The radial unwrapping of each image, shown below the image, indicates the degree of blurring in its perimeter. The line is the location determined by the analysis software to be the edge of the ball. Images of the silicon ball were obtained with it shifted both toward and away from the objective lens by up to 85 μm [Fig. 151.39(b)] in 17-μm steps. The focus control on the objective was not adjusted to compensate for the shift. The measured OD was reproduced within ± 0.5 μm of its average of 867.4 μm for all of the images.

This test was repeated, but this time the focus control on the objective *was* adjusted to compensate for the shift. The remeasured OD was reproduced within ± 0.5 μm of its average of 868.4 μm for all of the images; this time the average was 1 μm larger, most likely because of the lack of telecentricity of the objective lens.

To test the operator's reproducibility to refocus the objective lens, the Si ball was centered in the layering sphere and the objective's focus knob was turned to produce a noticeably out-of-focus image. An image was taken, the objective was refocused, and a second image was taken. This was repeated 15 times and the OD of the refocused images had an average of 867.4 μm with a standard deviation of ± 0.2 μm. The analysis software is surprisingly robust in that it underreported the OD by up to 6 μm, even for the grossly out-of-focus images [Fig. 151.39(c)]. Figures 151.39(a) and 151.39(b) demonstrate that the OD can be reproduced exactly, even when slightly unfocused.

Images of the PAMS capsule were also obtained with it shifted both toward and away from the objective lens by up to

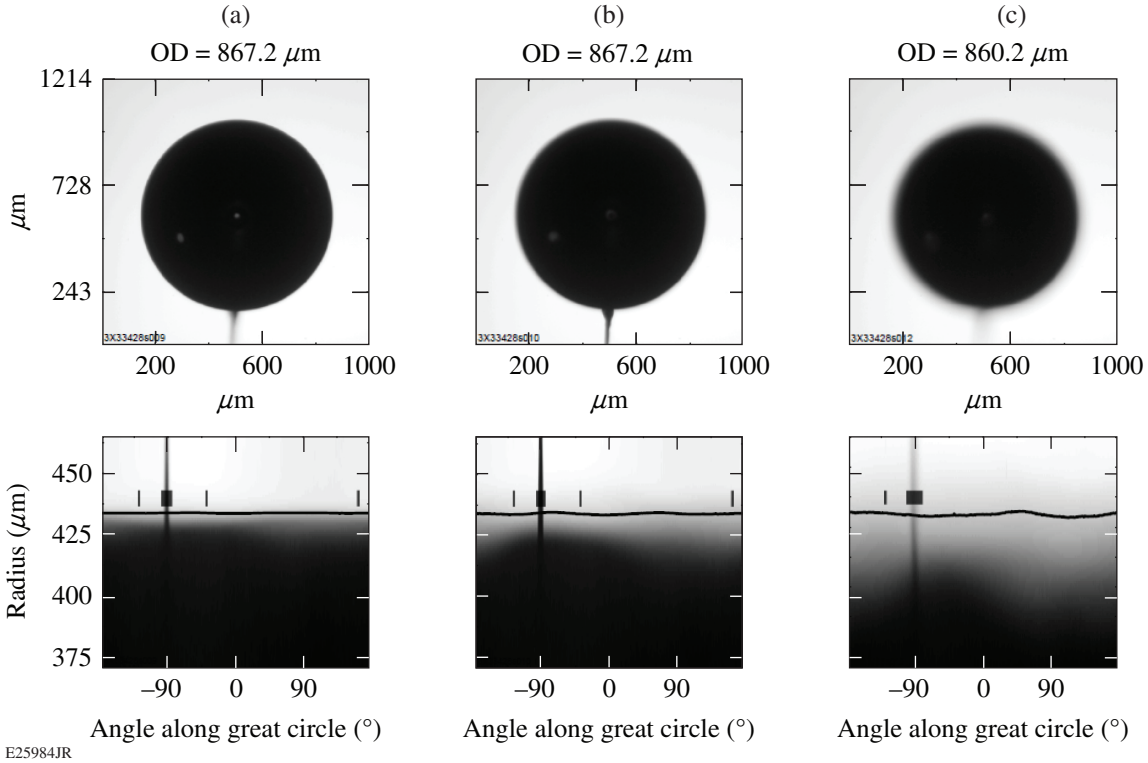

Figure 151.39

Several images taken during the focus scan: (a) Si ball at focal plane; (b) 85 μm away from focal plane; and (c) deliberately out of focus. The radial unwrapping of each image, shown below the image, indicates the degree of blurring in its perimeter. The line is the location determined by the analysis software to be the edge of the ball. Note that the blurring also overestimates the asymmetry of the capsule's OD, as indicated by the increased undulation of the line.

45 μm. In this test, the focus control on the objective was not adjusted to compensate for the shift. The measured OD's were reproduced within ±0.5 μm of their average of 869.2 μm for all of the images.

A lineout along the diameter would allow the operator to more objectively determine best focus in real time. However, the OD measurement is not sensitive to being slightly out of focus, certainly within the operator's qualitative ability to choose the correct focus.

4. Lateral Shift from Center

Since a cryogenic target is often vibrating both in and out of focus and laterally in the image during data acquisition, the sensitivity of the OD measurement to a lateral shift in the field of view was tested. As the capsule was shifted toward and away from the lens along the *x* axis in the focus-scan test, images were recorded along the *y* axis to determine if the measured OD changed with lateral position in the field of view. No difference in OD was measured even at extremes in lateral shift.

5. Characterization Station

The Cryogenic Target Facility contains three identical Characterization Stations. The Si ball was imaged in the same Moving Cryostat Transport Cart (MCTC) in all three stations; each was adjusted to the same illumination and focus conditions. The results are shown in Table 151.III. There was no statistical difference in OD measurement among the three stations.

6. Moving Cryostat Transfer Cart

During cryogenic target experiments, the capsule is stored, layered, transported, and characterized in a cryostat contained in a MCTC.[6] There is some slight variation in window thickness and alignment between the layering spheres in these carts. The data shown in Table 151.III were taken with the Si ball in MCTC #2. The ball was transferred into MCTC #7 and characterized at Characterization Station #3. Using the same illumination and focus conditions, no difference was observed between the measurements made in each cart.

Table 151.III: Comparison of the outside diameter of the Si ball measured at the three different Characterization Stations. The GA-measured OD = 864.1±0.5 μm, which is 3 μm less than the average of 866.8±0.3 μm for both axes shown here.

Characterization Station	*x*-axis OD (μm)	*y*-axis OD (μm)
1	867.0	867.4
2	866.2	866.8
3	866.6	866.8
Mean±σ	866.6±0.3	867.0±0.3

7. Warm Versus Cold Layering Sphere

The Si ball was cooled to 19 K in MCTC #2 at Characterization Station #3 and remeasured. The OD shrunk by, at most, 0.4 μm, as expected from the small thermal expansion coefficient of silicon. There was no statistical difference between the room-temperature and cryogenic measurements.

Data Analysis

1. Contraction of Cold, Unfilled, and D_2-filled Capsules

Images of two cold, unfilled GDP capsules were taken at 90° rotation intervals along both the *x*- and *y*-axis views, and the average OD was determined from each. These data, summarized in Table 151.IV, indicated that GDP capsules *do* contract when cooled; the difference being that they were

Table 151.IV: Change in OD after cooling from 293 K to 19 K for a sample of GDP shells that have *not* been exposed to DT. (The cold OD was reduced by 3 μm from the actual measurement to correct for the systematic error revealed during calibration testing.) The average change is 12.9±0.3 μm as expected from the thermal contraction calculated from the coefficient of thermal expansion and the temperature change.[12]

Capsule Type	Target Number	Outer Diameter (μm)				Average change (μm, corrected)	Percent change (corrected)
		Warm *x* axis	Warm *y* axis	Cold *x* axis	Cold *y* axis		
Unfilled GDP	CRYO-ME-4Q13-12	868.8	871.2	859.0	861.6	12.7	1.46
	CRYO-ME-4Q13-8	877.7	876.6	867.2	866.8	13.2	1.50
D_2-filled GDP	CRYO-2123-19-04	871.6		861.7		12.9	1.48
Mean±σ						12.9±0.3	1.48±0.03

never exposed to high-pressure DT, unlike the GDP capsules imploded during cryogenic target experiments that showed no contraction.

In addition, a single data point was obtained for a D_2-filled GDP capsule that also exhibited contraction. Although, since D_2 cryogenic target experiments have not been performed on OMEGA for many years, the fact that it contracted the same as the unfilled GDP capsule indicates that it is not mechanical stress from pressurization that causes the cold, DT-filled capsules' OD's to remain close to their room-temperature value.

2. Lack of Contraction of Cold, DT-filled Capsules

Past cryo target data were extracted from the database to compare warm versus cold OD's as a function of fill date, fuel-layer thickness, Characterization Station number, and MCTC number. These data represent 129 different capsules over a time period from 26 August 2014 to 8 December 2015; they are shown in increasing change in OD in Fig. 151.40. The warm OD's (measured by GA) and cold OD's (measured at the Characterization Stations) differ, on average, by 0.06±1.2 μm or 0.01±0.13%. Note that the 3-μm systematic error was not corrected in these data.

The possibility that a step change in measurement accuracy took place at some time in the recent past was explored; these data are shown in Fig. 151.41(a). The data on OD change are also plotted versus Characterization Station number [Fig. 151.41(b)] and MCTC number [Fig. 151.41(c)]. There is no clear trend in any of these data.

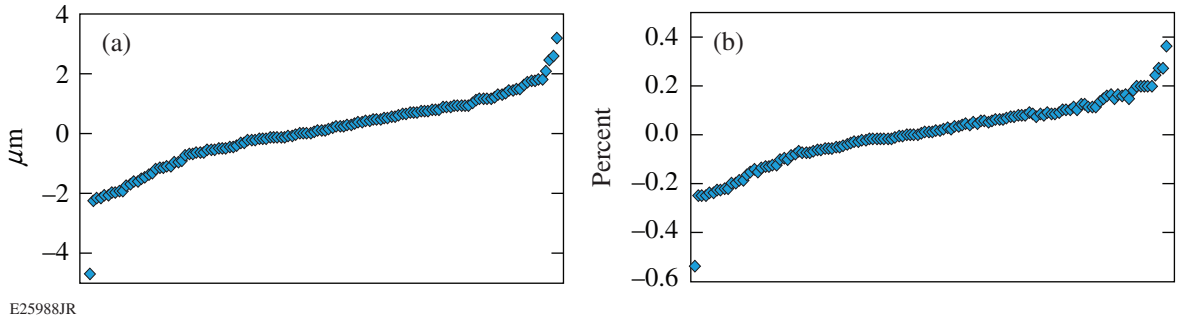

Figure 151.40
LLE's cold OD subtracted from GA's warm OD for 129 capsules, with the order shown in increasing difference: (a) the absolute change and (b) the percentage change. On average, they differ by 0.06±1.2 μm or 0.01±0.13%, respectively.

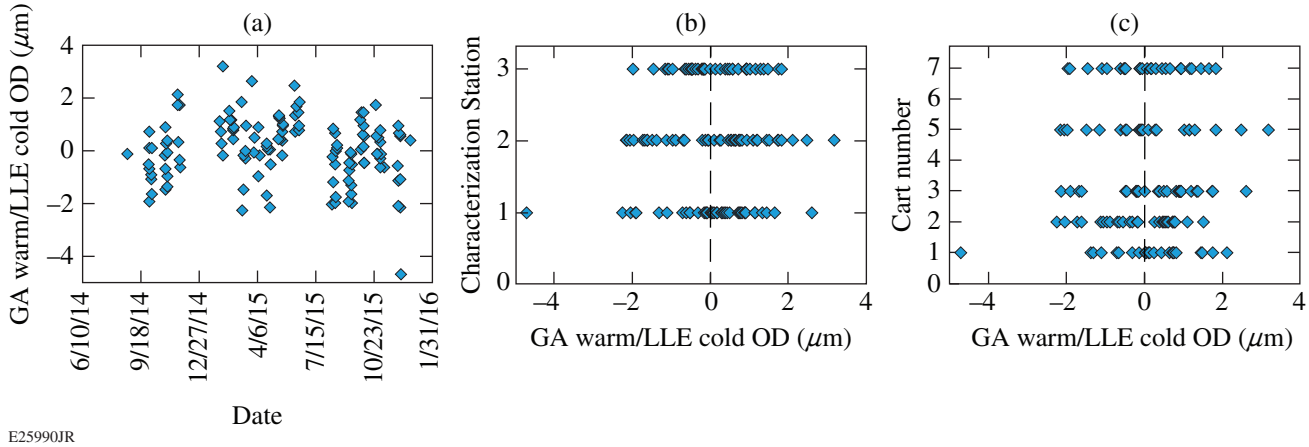

Figure 151.41
Change in outside diameter versus (a) measurement date, (b) Characterization Station number, and (c) MCTC number. There is no clear trend in any of these data; the data are scattered evenly around zero change. MCTC: Moving Cryostat Transfer Cart.

3. Contraction of a Nonpermeation-Filled Capsule

In an unrelated experiment,[7] a single GDP capsule with a 30-μm-diam hole laser-drilled in its wall was included in a permeation fill along with capsules of similar dimensions. Although not the original purpose of that experiment, the data from it can be used to evaluate if mechanical stresses from pressure gradients across the capsule are responsible for the lack of contraction of GDP capsules at cryogenic temperatures. The hole allows the GDP layer to be exposed to the same beta-decay bombardment inside and outside the capsule's wall in addition to that from tritium in solution within the wall, but without the mechanical stresses of the external pressure that enables permeation. The cold diameter was 3 μm less than a typical capsule that was permeation filled in the same batch, but this difference is not statistically significant compared with the range of changes exhibited in the ensemble of capsules shown in Fig. 151.40. A 3-μm-OD change falls within 2.5× the standard deviation from the nearly zero average OD change; if the sample of capsules was normally distributed, 98.8% of the OD-change values would also lie within 2.5 standard deviations from the mean.

Conclusions

The outside diameters of a silicon ball and two GDP capsules were measured while varying the illumination intensity, illumination geometry, focus shift, position of the capsule along the optical axis of the imaging system, position of the capsule laterally in the field of view, the Characterization Station, and MCTC. The greatest effect on OD measurement was illumination intensity, i.e., saturation of the image around the perimeter of the capsule. In addition, if the peak brightness of the illumination does not coincide with the optical axis and capsule center, intensity variations around the perimeter can locally affect where the analysis software determines the capsule's edge. Unsaturated images reproduced the OD measurement even under low illumination. Secondly, focus does have an effect on the OD, but errors are produced only if the image is noticeably out of focus.

A systematic overestimation of the OD was revealed during this study; overall, the Characterization Station–measured OD was greater by ~3 μm than that measured at GA. The capsule data acquired during this study corrected for this offset; however, the historic data collected from our database did *not* correct for this offset since the offset had existed for some unknown time and comparison of historical data must include it. The ~13-μm lack of observed contraction was not a result of measurement error—the systematic error can account for only 3 μm; the remaining effect is real.

The OD's of three GDP capsules that had *not* been exposed to DT were measured at both room temperature and 19 K. After the data were corrected for the 3-μm systematic error, they all contracted by 13 μm, which is 1.5% of their warm OD, as expected. A database comparison of 129 DT-filled capsules revealed that they contracted by an average of 0.06±1.2 μm or 0.01±0.13%. A lack of the ~10-μm anticipated contraction and the overmeasurement of the OD by 2 to 3 μm can explain the up-to-13-μm, larger-than-expected OD's reported by the measurement software.

Radiation damage to the polymer while exposed to beta-particle bombardment during DT permeation[7] explains the lack of contraction. GDP capsules are a highly cross-linked polymer.[8] The average beta-particle energy from tritium decay is 5.7 keV—strong enough to break multiple molecular bonds in the polymer that are a few eV each. Therefore, broken carbon–carbon bonds can readily bond with the ionized hydrogen dissolved in the wall of the capsule. We postulate that the capsules, therefore, swell during permeation to a degree that is nearly compensated for by the contraction during cooling.

Conversely, polystyrene exhibits a high resistance to radiation damage: the polystyrene capsules experience less damage during permeation and contract as expected when cooled, as shown in Table 151.V. Polymers containing aromatic molecules generally are much more resistant to radiation degradation than are aliphatic polymers; this is true whether or not the aromatic group is directly in the chain backbone. Consequently polystyrenes, with a pendant aromatic group, and polyimides, with an aromatic group directly in the polymer backbone, are relatively resistant to high doses of radiation (>4000 kGy) (Refs. 9 and 10).

The GDP capsules containing thicker layers were exposed to DT for a longer period and at a higher concentration during permeation, yet there is no strong correlation of OD change with layer thickness (see Fig. 151.42). There is a possible shift in the median in the data toward less shrinkage as the layer thickness increases, but it is not a convincing trend. This would imply that damage and swelling occur early in the process and conclude quickly.

A DT-gas sample retrieved from the permeation cell following GDP capsule permeation was sent to LLNL to be analyzed with their magnetic-sector mass spectrometer.[11] Many of the constituents in the sample were light hydrocarbons as shown in Fig. 151.43. Since the DT delivery system is constructed of stainless-steel tubing joined by either welded or metal-sealed

Table 151.V: Change in OD after cooling from 293 K to 19 K for a sample of DT-filled polystyrene shells. (The cold OD was reduced by 3 μm from the actual measurement to correct for the systematic error revealed during calibration testing.) The average percent change is 1.11±0.12%, close to the 1.44% thermal contraction calculated from the coefficient of thermal expansion and the temperature change.[12]

Target Number	Outer Diameter (μm)			Warm to Cold (μm, corrected)	Percent Change (corrected)
	Warm	Cold	Cold (corrected)		
CRYO-9079-18	875.0	868.8	865.8	9.2	1.05
CRYO-9083-12	869.0	862.4	859.4	9.6	1.10
CRYO-9089-37	868.0	860.4	857.4	10.6	1.22
CRYO-9088-38	867.0	858.6	855.6	11.4	1.31
CRYO-9089-34	869.0	860.3	857.3	11.7	1.35
CRYO-9116-0021	960.2	952.8	949.8	10.4	1.08
CRYO-9114-0018	962.8	954.0	951.0	11.8	1.23
CRYO-9112-0020	963.4	956.1	953.1	10.3	1.07
CRYO-9107-0023	967.4	959.9	956.9	10.5	1.09
CRYO-9107-0017	967.4	960.7	957.7	9.7	1.00
CRYO-9080-0029	872.0	866.6	863.6	8.4	0.96
CRYO-9080-0034	872.0	865.7	862.7	9.3	1.07
CRYO-9077-0035	878.4	872.4	869.4	9.0	1.02
CRYO-9079-0042	874.8	868.5	865.5	9.3	1.06
CRYO-9080-0041	876.0	870.3	867.3	8.7	0.99
Mean±σ				10.0±1.1	1.11±0.12

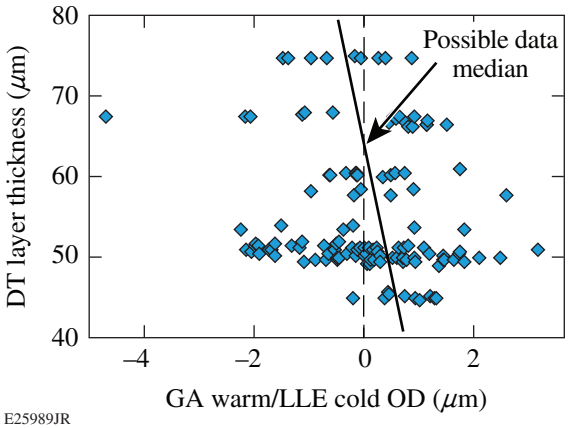

Figure 151.42
Change in outside diameter versus final layer thickness. There is no convincing trend in these data; however, a possible slanting median to the data may indicate less shrinkage with increasing DT exposure.

fittings and the target support is constructed of non-carbon-containing materials (aside from several small polymeric glue joints), total tritiated hydrocarbons in the 1000-ppm range suggest radiation-induced damage to the GDP during permeation, reinforcing the above conclusion regarding swelling prior to contraction during cooling.

ACKNOWLEDGMENT

This material is based upon work supported by the Department of Energy National Nuclear Security Administration under Award Number DE-NA0001944, the University of Rochester, and the New York State Energy Research and Development Authority.

REFERENCES

1. T. C. Sangster, R. Betti, R. S. Craxton, J. A. Delettrez, D. H. Edgell, L. M. Elasky, V. Yu. Glebov, V. N. Goncharov, D. R. Harding, D. Jacobs-Perkins, R. Janezic, R. L. Keck, J. P. Knauer, S. J. Loucks, L. D. Lund, F. J. Marshall, R. L. McCrory, P. W. McKenty, D. D.

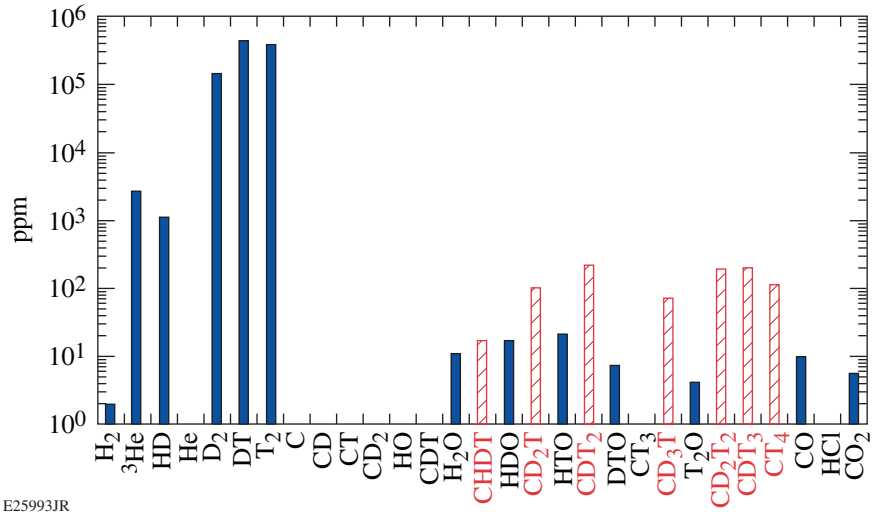

Figure 151.43
A magnetic-sector mass spectrogram of the constituents in a DT-gas sample retrieved from the permeation cell following glow-discharge plasma (GDP) capsule permeation. A significant fraction of the gas is composed of light hydrocarbons (shown in the red crosshatched bars) that have been released from the CH capsule during permeation.

Meyerhofer, P. B. Radha, S. P. Regan, W. Seka, W. T. Shmayda, S. Skupsky, V. A. Smalyuk, J. M. Soures, C. Stoeckl, B. Yaakobi, J. A. Frenje, C. K. Li, R. D. Petrasso, F. H. Séguin, J. D. Moody, J. A. Atherton, B. D. MacGowan, J. D. Kilkenny, T. P. Bernat, and D. S. Montgomery, Phys. Plasmas **14**, 058101 (2007).

2. O. A. Hurricane, D. A. Callahan, D. T. Casey, E. L. Dewald, T. R. Dittrich, T. Döppner, M. A. Barrios Garcia, D. E. Hinkel, L. F. Berzak Hopkins, P. Kervin, J. L. Kline, S. Le Pape, T. Ma, A. G. MacPhee, J. L. Milovich, J. Moody, A. E. Pak, P. K. Patel, H.-S. Park, B. A. Remington, H. F. Robey, J. D. Salmonson, P. T. Springer, R. Tommasini, L. R. Benedetti, J. A. Caggiano, P. Celliers, C. Cerjan, R. Dylla-Spears, D. Edgell, M. J. Edwards, D. Fittinghoff, G. P. Grim, N. Guler, N. Izumi, J. A. Frenje, M. Gatu Johnson, S. Haan, R. Hatarik, H. Herrmann, S. Khan, J. Knauer, B. J. Kozioziemski, A. L. Kritcher, G. Kyrala, S. A. Maclaren, F. E. Merrill, P. Michel, J. Ralph, J. S. Ross, J. R. Rygg, M. B. Schneider, B. K. Spears, K. Widmann, and C. B. Yeamans, Phys. Plasmas **21**, 056314 (2014).

3. B. A. Vermillion *et al.*, Fusion Sci. Technol. **51**, 791 (2007).

4. D. D. Meyerhofer, R. S. Craxton, L. M. Elasky, D. R. Harding, R. L. Keck, M. Pandina, W. Seka, M. D. Wittman, A. Warrick, and T. G. Brown, Bull. Am. Phys. Soc. **48**, 55 (2003).

5. APPLIED IMAGE Inc., Rochester, NY 14609.

6. G. E. Besenbruch *et al.*, in *Inertial Fusion Sciences and Applications 99*, edited by C. Labaune, W. J. Hogan, and K. Tanaka (Elsevier, Paris, 2000), pp. 921–926.

7. D. R. Harding and W. T. Shmayda, Fusion Sci. Technol. **63**, 125 (2013).

8. B. W. McQuillan *et al.*, Fusion Technol. **31**, 381 (1997).

9. Polymer Materials Selection for Radiation-Sterilized Products, Medical Device and Diagnotic Industry, http://www.mddionline.com/article/polymer-materials-selection-radiation-sterilized-products (accessed 3 August 2017).

10. D. A. Badenhorst, presented at the Ninth National Conference of the South African Section of the PRI, Johannesburg, South Africa, 22–23 October 1987 (Paper C18).

11. P. S. Ebey *et al.*, Fusion Sci. Technol. **49**, 859 (2006).

12. CryoComp 5.0 for Windows User Manual, Eckels Engineering Inc., Florence, SC 29501.